JCTC Journal of Chemical Theory and Computation

Article

pubs.acs.org/JCTC

Evaluating the Accuracy of Hessian Approximations for Direct Dynamics Simulations

Yu Zhuang,*[,†] Matthew R. Siebert,[‡] William L. Hase,[‡] Kenneth G. Kay,[§] and Michele Ceotto*[,∥]

[†]Department of Computer Science, Texas Tech University, Lubbock, Texas 79409-3104, United States

[‡]Department of Chemistry and Biochemistry, Texas Tech University, Lubbock, Texas 79409, United States

[§]Department of Chemistry, Bar-Ilan University, Ramat-Gan 52900, Israel

[∥]Dipartimento di Chimica, Università degli Studi di Milano, via Golgi 19, 20133 Milano, Italy

ABSTRACT: Direct dynamics simulations are a very useful and general approach for studying the atomistic properties of complex chemical systems, since an electronic structure theory representation of a system's potential energy surface is possible without the need for fitting an analytic potential energy function. In this paper, recently introduced compact finite difference (CFD) schemes for approximating the Hessian [*J. Chem. Phys.* **2010**, *133*, 074101] are tested by employing the monodromy matrix equations of motion. Several systems, including carbon dioxide and benzene, are simulated, using both analytic potential energy surfaces and on-the-fly direct dynamics. The results show, depending on the molecular system, that electronic structure theory Hessian direct dynamics can be accelerated up to 2 orders of magnitude. The CFD approximation is found to be robust enough to deal with chaotic motion, concomitant with floppy and stiff mode dynamics, Fermi resonances, and other kinds of molecular couplings. Finally, the CFD approximations allow parametrical tuning of different CFD parameters to attain the best possible accuracy for different molecular systems. Thus, a direct dynamics simulation requiring the Hessian at every integration step may be replaced with an approximate Hessian updating by tuning the appropriate accuracy.

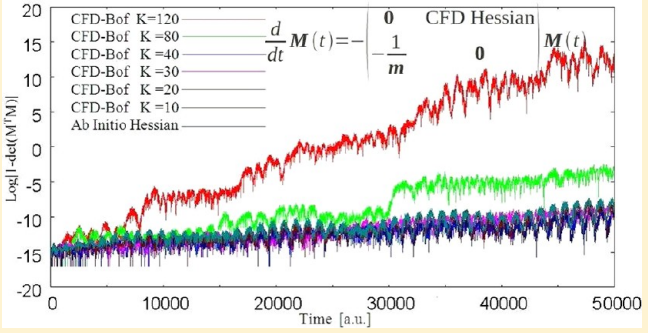

1. INTRODUCTION

Classical chemical[1,2] and molecular[3] dynamics simulations are widely employed to study molecular processes.[4,5] With increased computational power, simulations representing thousands of atoms are possible.[6−9] The simulations range from a single-trajectory molecular dynamics description of a complex system[10−13] to an ensemble with thousands of trajectories for the statistical averaging of chemical dynamics.[14,15] Classical trajectories are also used within the path integral formulation of quantum mechanics[16−26] and within the semiclassical approximation of quantum mechanics.[27−42] For each of these studies, it is very important to know how to evaluate the accuracy of a classical trajectory's time evolution.

The accuracy of a classical trajectory is established by the accuracy of its atomic-level motions.[1] The energy conservation of a single trajectory is often considered as the way to test the accuracy of classical time evolution. Surely this is a fast and easy approach. However, it gives only a partial view of the problem, since it cannot distinguish between a symplectic propagator[43−46] and a nonsymplectic one. The issue is not marginal, since the classical time evolution is a canonical transformation and, therefore, must be symplectic.[47] The calculation of the monodromy matrix determinant[48] provides a simple and useful check for the accuracy of the classical trajectory evolution. The Hessian of the potential energy surface (PES) is required, and any numerical error in the Hessian calculation will be detected as a deviation of the determinant from unity, as explained in Appendix I.

The computational cost of the Hessian increases rapidly with dimensionality and an approximation to the Hessian for some integration time steps makes obtaining the Hessian in a classical trajectory calculation more practical. Thus, the monodromy matrix represents a tool to check not only whether positions and moments are canonically evolved but also whether a Hessian approximation is accurate. This last restriction is somehow a higher order check of the classical evolution than energy conservation, since it involves second derivatives of the potential. In a follow-up paper,[49] we show that for a semiclassical dynamics simulation, where thousands of trajectories are usually required, it is possible to approximate the Hessian, which significantly reduces the computational cost of semiclassical dynamics. In these cases, monitoring the monodromy matrix determinant is essential for establishing the accuracy of the Hessian approximation.

The traditional approach for performing a classical dynamics simulation is based on a fitted analytic PES or a model force field. Fitting an analytic potential energy function to electronic structure theory calculations becomes quite cumbersome and subtle when the dimensionality increases and the system becomes more complex. The resulting analytic potential and its derivatives may differ significantly from the exact ones due to the fitting

Received: July 6, 2012
Published: November 13, 2012

procedure. To remove any doubt about the accuracy of the fitting to the electronic structure theory energies, one can estimate the fidelity overlap.[34,35] Moreover, the accuracy of fitting first and higher potential derivatives should be tested as well. Unfortunately, this is not an easy task, which makes it difficult to assess the accuracy of the Hessian.

A more general approach for a classical dynamics simulation is direct dynamics, for which the potential and its derivatives are obtained directly "on-the-fly" from an electronic structure theory. Direct dynamics avoids the need to fit an analytic PES or use a model PES, and direct dynamics[5,50−54] has become an important simulation tool for an increasing number of problems, ranging from chemistry to materials science and biology. For some electronic structure theories and computer programs, the Hessian may be obtained directly. However, the computational cost of a Hessian calculation at each time-step of a direct dynamics simulation can sometimes turn out to be prohibitive. Thus, it is important to have robust and trustworthy algorithms for approximating the Hessian and estimating the accuracy of the approximations. This is the reason why the monodromy matrix calculation is important, since it allows one to check the accuracy of the Hessian approximation without the need to calculate the exact Hessian.

Of the different ways to perform a direct dynamics simulation,[50,52,55,57−59,64,65] Born−Oppenheimer direct dynamics is one of the most accurate, since the atomic positions are propagated by forces that are calculated for the adiabatic electronic state at each instantaneous arrangement of the atoms. Nevertheless, the time reversibility and symplecticity have been questioned, because of the irreversible and nonlinear nature of the SCF optimization part of the electronic structure theory calculation.[52,55,56] This problem may be overcome with the construction of time-reversible Born−Oppenheimer direct dynamics methods,[57−59] where a Lagrangian formalism is properly extended to the electronic degrees of freedom and without any fictitious mass dependency.[60−63]

The Hessian approximation tested in this paper represents a potential significant computational savings for semiclassical direct dynamics,[66−72] where the Hessian calculation is mandatory for the prefactor of the quantum propagator, as for semiclassical initial value representation methods.[73] Hessian update schemes were originally developed for optimizations (see refs 74−79 and references therein) and some have been used in direct dynamics simulations.[80,81,83] Most of the schemes are based on a first-order Taylor expansion which, for optimizations, provides the basis for quasi-Newton methods. The accuracy of the first-order Taylor expansion is sufficient for optimizations, as evidenced by the fast convergence of some of the quasi-Newton methods.[76] However, for direct dynamics, higher accuracy is desirable, and a recent study[82] illustrated the effectiveness of highly accurate Hessian approximations for attaining high quality simulations. The Hessian approximation schemes[82] were developed using compact finite difference (CFD),[84−88] which has an approximation accuracy one order higher than that of the first-order Taylor expansion. Multiple CFD-based Hessian approximation schemes were derived,[82] and two of the schemes, the CFD-Bofill and the CFD-PSB schemes, are among the best in terms of simplicity and accuracy.

In this paper, we use the monodromy matrix for checking the accuracy of the CFD approximation for both analytic potential and on-the-fly classical dynamics simulations. The CFD approximation is reviewed in section 2. Then, the monodromy matrix definition and properties are discussed in section 3. In the same section, as well as in Appendix I, the usage of the monodromy matrix to evaluate the accuracy of the Hessian calculation is explained. Simulation results are presented in section 4 and summarized in section 5.

2. THE CFD APPROXIMATION FOR HESSIAN CALCULATIONS

Compact finite difference (CFD) is a high-order finite difference approximation of differentiations of functions without incurring a large stencil (the set of sampling points in the approximation formula).[84−88] Higher accuracy is attained by including differentiated terms at more locations within the stencil. The "compact" refers to the compactness of the stencil for attaining high-accuracy approximation.

The CFD-based Hessian approximations start with the equation[82]

$$\frac{1}{2}[H(X_1) + H(X_2)](X_2 - X_1) = G(X_2) - G(X_1) \tag{1}$$

where $G(X_1)$ and $G(X_2)$, respectively, are the gradients of the potential energy at X_1 and X_2, and $H(X_1)$ and $H(X_2)$ are the respective Hessians at X_1 and X_2. Compared with the first-order Taylor expansion

$$H(X_2)(X_2 - X_1) = G(X_2) - G(X_1) \tag{2}$$

of $G(X_1)$ about the point X_2, the CFD-based eq 1 has an error of $O(\|X_1 - X_2\|^3)$ while the Taylor expansion in eq 2 has an error of $O(\|X_1 - X_2\|^2)$. Note that eq 1 has the same stencil as eq 2, but with the Hessian included at one more location of the variable X. When $G(X_1)$, $G(X_2)$, and $H(X_1)$ are given, a Hessian update scheme is to approximate $H(X_2)$ using the given information of $G(X_1)$, $G(X_2)$, $H(X_1)$, and X_1 and X_2. Equation 2 is the equation on which most of the existing Hessian update schemes are based. When the variable X is a vector with n scalar entries, that is, $X = (x_1, x_2, ..., x_n)$, both eqs 1 and 2 have an $n(n-1)/2$-dimensional solution space. A dimension-restriction technique pioneered by Bofill,[79] originally for the first-order eq 2, can be applied to the CFD eq 1, with which one can obtain a family of Hessian update schemes:

$$\Delta H = (1-\lambda)\frac{RR^T}{R^T\Delta X} + \lambda\left(\frac{\Delta X R^T + R\Delta X^T}{\|\Delta X\|^2} - \frac{R^T\Delta X}{\|\Delta X\|^4}\Delta X\Delta X^T\right) \tag{3}$$

from which $H(X_2)$ can be obtained using $H(X_2) = H(X_1) + \Delta H$, where λ is a parameter allowed to vary, $\Delta X = X_2 - X_1$, and

$$R = 2[G(X_2) - G(X_1) - H(X_1)(X_2 - X_1)] \tag{4}$$

Equation 3 is called the CFD-Bofill family[82] of Hessian update schemes, where the CFD contribution is effected through eq 4 for R. Equation 3 becomes the CFD-symmetric rank-one (CFD-SR1) scheme (see ref 76) when $\lambda = 0$ and reduces to the CFD-Power Symmetric Broyden (CFD-PSB) scheme when $\lambda = 1$. Thus, the CFD-Bofill family of schemes can be viewed as linear combinations of the CFD-SR1 and CFD-PSB schemes. It is worth noting that when R is half of eq 4, that is, $R = G(X_2) - G(X_1) - H(X_1)(X_2 - X_1)$, eq 3 gives the family of CFD-Bofill update schemes that are solutions of the first-order eq 2.

All schemes of the form in eq 3 are solutions of eq 1, which means that they are exactly the same when multiplied by $X_2 - X_1$. Hence differences among update schemes of the form in eq 3 must be on the subspace orthogonal to $X_2 - X_1$,

dx.doi.org/10.1021/ct300573h | J. Chem. Theory Comput. 2013, 9, 54−64

i.e., the orthogonal complement of $X_2 - X_1$. Studies (see ref 78 and references therein) show that the SR1 scheme produces very fast convergence for optimization if $R^T\Delta X$ stays away from 0 but suffers from large error when R and ΔX are mutually orthogonal or nearly mutually orthogonal. This suggests that when compared with other schemes, SR1 might be a good approximation of the Hessian in the orthogonal complement of $X_2 - X_1$ when its denominator stays away from zero. A practical value for λ that is due to Bofill[79] is

$$\lambda = 1 - \frac{(R^T\Delta X)^2}{\|R\|^2 \cdot \|\Delta X\|^2} \tag{5}$$

With this choice for λ, eq 3 is guaranteed to stay away from division by near-zero, since the numerator of $1 - \lambda$ cancels with $R^T\Delta X$, the denominator of the CFD-SR1 scheme. The CFD-Bofill update scheme given by eq 3 with eq 5 for λ was reported to be a simple and accurate Hessian approximator[82] and is one of the two schemes used for the dynamics simulations reported in section 4. The other simple and accurate update scheme also used in the simulations is the CFD-PSB Hessian update scheme, that is, $\lambda = 1$ in eq 3.

3. EVALUATING THE ACCURACY OF APPROXIMATED HESSIANS

Numerical accuracy for a classical trajectory time integration is usually determined by monitoring the energy conservation. However, in order to see how a small perturbation introduced by a numerical approximation is propagated in time, a different approach may be taken.

Here, we recall the equations of motion of the monodromy matrix, focusing on their interpretation in terms of the separation of nearby classical trajectories. When two classical trajectories are infinitesimally close to each other at the starting phase space point and then evolved with time t, the phase space separation of the trajectories is given by the following set of equations:

$$\begin{cases} \delta\mathbf{p}_t(\mathbf{p}_0, \mathbf{q}_0) = \dfrac{\partial \mathbf{p}_t}{\partial \mathbf{p}_0}\delta\mathbf{p}_0 + \dfrac{\partial \mathbf{p}_t}{\partial \mathbf{q}_0}\delta\mathbf{q}_0 \\ \delta\mathbf{q}_t(\mathbf{p}_0, \mathbf{q}_0) = \dfrac{\partial \mathbf{q}_t}{\partial \mathbf{q}_0}\delta\mathbf{q}_0 + \dfrac{\partial \mathbf{q}_t}{\partial \mathbf{p}_0}\delta\mathbf{p}_0 \end{cases} \tag{6}$$

where $(\delta\mathbf{p}_0, \delta\mathbf{q}_0)$ are the initial separations in phase space and $(\delta\mathbf{p}_t, \delta\mathbf{q}_t)$ are the final ones. Equation 6 can be written in a more compact form by introducing the so-called (stability) monodromy matrix[48]

$$\mathbf{M} = \begin{pmatrix} m_{\mathbf{pp}} & m_{\mathbf{pq}} \\ m_{\mathbf{qp}} & m_{\mathbf{qq}} \end{pmatrix} \tag{7}$$

where, for example, the block element $m_{\mathbf{pq}}$ is

$$m_{\mathbf{pq}} = \begin{pmatrix} \dfrac{\partial p_1(t)}{\partial q_1(0)} & \cdots & \dfrac{\partial p_1(t)}{\partial q_N(0)} \\ \cdots & \cdots & \cdots \\ \dfrac{\partial p_N(t)}{\partial q_1(0)} & \cdots & \dfrac{\partial p_N(t)}{\partial q_N(0)} \end{pmatrix} \tag{8}$$

and the partial derivatives are for each momentum at time t with respect to each initial position. N is the number of degrees of freedom, and the dimension of the monodromy matrix is $2N \times 2N$. By introducing eq 7 into eq 6, the final phase space separation becomes

$$\begin{pmatrix} \delta\mathbf{p}_t \\ \delta\mathbf{q}_t \end{pmatrix} = \begin{pmatrix} m_{\mathbf{pp}} & m_{\mathbf{pq}} \\ m_{\mathbf{qp}} & m_{\mathbf{qq}} \end{pmatrix} \begin{pmatrix} \delta\mathbf{p}_0 \\ \delta\mathbf{q}_0 \end{pmatrix} \tag{9}$$

Given the classical Hamiltonian for N degrees of freedom

$$H(\mathbf{p}_t, \mathbf{q}_t) = \sum_{i=1}^{N} \frac{p_i^2(t)}{2m} + V(q_1(t), \ldots, q_N(t)) \tag{10}$$

at each time t and assuming the same mass m for each degree of freedom without a loss of generality, the momenta and positions separations can be written as (see Appendix II)

$$\frac{d}{dt}\begin{pmatrix} \delta\mathbf{p}_t \\ \delta\mathbf{q}_t \end{pmatrix} = \mathbf{K}\cdot\mathbf{M}\begin{pmatrix} \delta\mathbf{p}_0 \\ \delta\mathbf{q}_0 \end{pmatrix} \tag{11}$$

where eq 9 has been used and

$$\mathbf{K} = \begin{pmatrix} 0 & -\dfrac{\partial^2 V(\mathbf{q})}{\partial \mathbf{q}^2} \\ \dfrac{1}{m} & 0 \end{pmatrix} \tag{12}$$

If eq 9 is derived with respect to time

$$\frac{d}{dt}\begin{pmatrix} \delta\mathbf{p}_t \\ \delta\mathbf{q}_t \end{pmatrix} = \frac{d}{dt}M\begin{pmatrix} \delta\mathbf{p}_0 \\ \delta\mathbf{q}_0 \end{pmatrix} \tag{13}$$

and equated to eq 11, then the time evolution of the monodromy matrix becomes

$$\frac{d}{dt}\mathbf{M}(t) = \mathbf{K}\cdot\mathbf{M}(t) \tag{14}$$

where the initial condition is the identity matrix as from the definition of eq 7. Key properties of the monodromy matrix are that its determinant is unity at the initial time and that this value is preserved under classical time evolution. The first property is easily verified by eqs 7 and 8. The second may be proven by either recognizing that the determinant of the monodromy matrix may be viewed as a Jacobian for the change of variables $(\mathbf{p}(t), \mathbf{q}(t)) \rightarrow (\mathbf{p}(t + dt), \mathbf{q}(t + dt))$ or a phase space area, and the conservation of the determinant is equivalent to stating that the trajectory is canonically integrated. This property is a direct consequence of Liouville's theorem.

The importance of introducing the mondromy matrix in the description of the classical motion is that one can detect any inaccuracies in the numerical integration of the classical equations of motion by calculating the determinant of this matrix at each time step. While the accuracy of the momenta and coordinates may be checked from the energy conservation, the Hessian matrix accuracy can be monitored by calculating the evolution of the monodromy matrix according to eq 14 and determining any deviation of the determinant from unity. The Hessian is part of the monodromy matrix time evolution, as shown by eqs 12 and 14. If the numerical approximation of the Hessian is poor, then the determinant of the monodromy matrix will quickly deviate from unity, as illustrated in Appendix I.

dx.doi.org/10.1021/ct300573h | J. Chem. Theory Comput. 2013, 9, 54−64

4. RESULTS

In this section, the accuracy of the CFD Hessian approximation is tested with simulations on analytic potentials and with Born−Oppenheimer direct dynamics. For the first, three types of analytic potentials are considered in order to exploit different kinds of couplings, resonances, etc. These are the potentials for water and carbon dioxide and the Henon−Heiles model. Direct dynamics simulations were performed for both carbon dioxide and benzene. These simulations for carbon dioxide were compared with those obtained with the analytic potential.

All the classical trajectory evolution algorithms used in this paper are symplectic ones. In order to construct a symplectic or geometric algorithm, the canonical time evolution is represented as a map. Then, a generating function, which must include mixed old and new phase space variables, is associated with the canonical transformation.[43] The full integration step is the complete sequence of maps. The number of intermediate values of positions and momenta within the map and between a time step and another is equal to the order of the integrator. These values of positions and momenta are merely for propagation convenience and should not be interpreted for physical evaluations. The symplectic coefficients of the integration algorithm are usually found by representing the map in the exponential form and then by breaking this down into products, using commutator relations.[43,44,46] In this way, one can derive the second-order velocity Verlet,[89] the fourth-order McLachlan,[90] and the sixth-order Blanes II[91] algorithms, and many others.[46,58]

For each simulation, the molecular geometry was first optimized and then the normal modes of vibration determined. Each trajectory is initialized at this potential energy minimum by adding an amount of kinetic energy to each normal mode equal to the mode's harmonic zero-point energy. For the calculations employing analytic potentials, the "exact" Hessian is calculated by finite difference using the second order central scheme and the first derivatives using the first order central scheme. For both, the space increment is 0.001 au in mass scaled coordinates. For the direct dynamics, the Hessian is obtained analytically and directly from electronic structure theories.

4.1. Simulations on Analytic Potentials. The performance of the CFD Hessian approximation was first investigated using integration algorithms of a different order for the same physical system. In the following set of simulations, the time increment has been set to 10 au and the number of time steps to 5000. In Figures 1, 2, and 3, the monodromy matrix evolution is performed for the water molecule using the velocity Verlet, the McLachlan, and the Blanes II algorithms, respectively. The analytic PES for water is from ref 92. In Figure 1, the black lines (red lines) in each panel describe the deviation of the monodromy matrix determinant from unity when the CFD-Bofill (CFD-PSB) approximation is adopted to evaluate the Hessian matrix for a number of K time steps. Thus, every K steps, the Hessian is again calculated numerically using potentials from the analytic potential energy function. The green lines are the exact deviations, i.e., those obtained by evaluating the Hessian at each time step. As described at the beginning of this section, in a geometric algorithm there are a number of intermediate steps, which are equal to the order of the algorithm. Thus, when K is set equal to one, the Hessian is approximated one time when a second order algorithm is used, three times for a fourth order, and six times for the Blanes II algorithm. Thus, for each panel in Figure 1, the number of times the CFD approximation is invoked is given by the values at $K = 1$ times the panel number K. For example, by using a velocity Verlet algorithm and $K = 8$, the Hessian is estimated every 16 time steps.

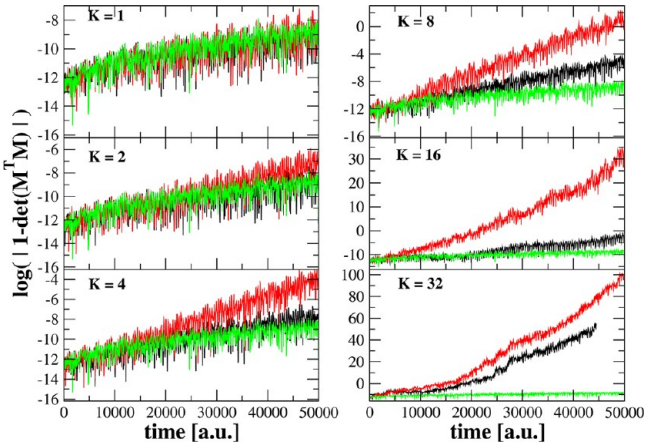

Figure 1. Deviation of the monodromy matrix determinant from unity at each time step. The second order symplectic velocity Verlet algorithm is employed. Each panel is for a different number K of interpolated time steps. The black line is the CFD-Bofill Hessian approximation; the red, the CFD-PSB one; and the green line, the exact value.

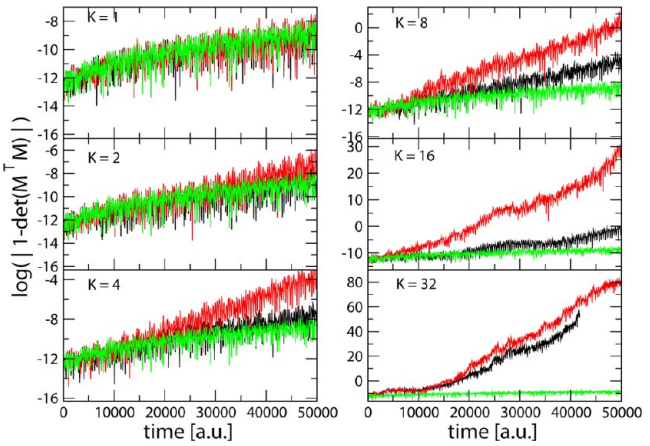

Figure 2. The same as in Figure 1 but for the fourth-order McLachlan symplectic algorithm.

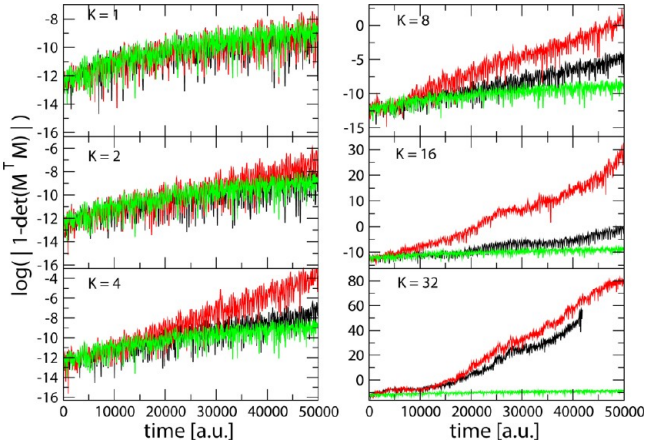

Figure 3. The same as in Figure 1 but for the sixth-order Blanes II symplectic algorithm.

dx.doi.org/10.1021/ct300573h | J. Chem. Theory Comput. 2013, 9, 54−64

Figure 1 shows how both CFD approximation errors are very much contained up to $K = 4$. When K is set equal to 8 and 16, the CFD-PSB approximation cannot be employed anymore, while the CFD-Bofill one is still quite accurate. When K is equal to 32, both approximations badly fail to describe the Hessian time evolution.

Figure 2 shows the same set of simulations as in Figure 1, but employing the fourth order McLachlan algorithm.[90] The trends are quite similar to those of Figure 1 and show that the CFD-Bofill approximation may be preferred as compared to the CFD-PSB one for strongly coupled molecules such as water. An important note about this second set of simulations regards the computational time. Given that the McLachlan algorithm is a fourth-order one, the computational time is a factor of 2 less as compared to that for the velocity Verlet. For example, for K equal to 8, the Hessian is calculated only once in every 32 steps and estimated for the other time steps.

Finally, Figure 3 reports the same set of calculations as in the previous figures but using the sixth-order geometric algorithm Blanes II. Both approximations behave quite the same as in the previous simulations, and the computational time is 3 times less than for the velocity Verlet simulations.

In order to appreciate the performance of the CFD approximations for different types of motions, a set of simulations on a carbon dioxide analytic PES is presented. This system is known for the Fermi resonance splittings occurring between the symmetric stretch and bending modes. For these reasons, it is considered a strongly coupled system. Here, the atoms involved in the motions are heavier than in a water molecule, and the time step is kept the same for direct comparison purposes.

In Figure 4, velocity Verlet CO_2 simulations are reported for an analytic PES,[66] and the color code employed is the same as

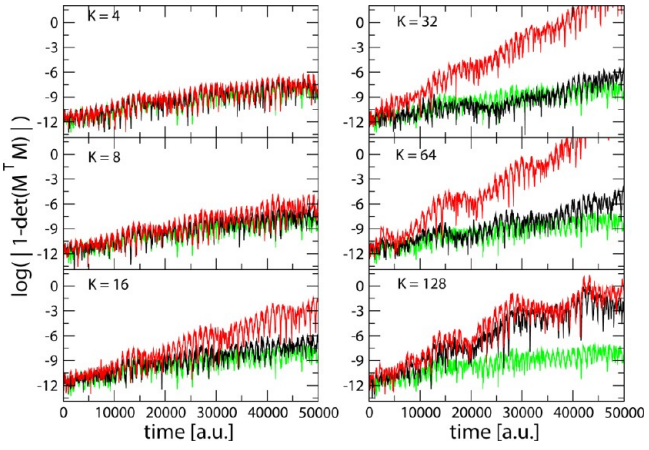

Figure 4. The same as in Figure 1, but for the carbon dioxide molecule. Two orders of magnitude computational time can be saved by employing the CFD Hessian approximation.

in previous figures. The CFD approximation is overall offering a more significant computational saving for this case. In particular, by fixing $K = 64$ and using the CFD-Bofill approximation, one can save about 2 orders of magnitude computational time in calculating the Hessian. Clearly this represents a significant boost when Born–Oppenheimer direct dynamics are employed. Once again the better performance of the CFD-Bofill approximation versus the CFD-PSB one is confirmed.

Finally, simulations are performed using the well-known chaotic Henon–Heiles potential. The potential equation

$$V(q_1, q_2, ..., q_N) = \frac{m\omega^2}{2}\sum_{i=1}^{N} q_i^2 + \lambda \sum_{i=1}^{N-1}\left(q_{i+1}q_i^2 - \frac{1}{3}q_{i+1}^3\right) \quad (15)$$

is a many-dimensional extension of the original Henon–Heiles one.[93] The values of the masses m and of the harmonic component ω of the potential have been fixed to $m = 914$ au and $\omega = 66$ cm^{-1} in order to reproduce a floppy system. The parameter λ is tuned in a way to introduce a significant amount of chaos into the oscillators' motion. The number of oscillators has been set to 10.

The goal of these simulations is to see if chaos can somehow ruin the accuracy of the CFD approximations. From the green lines in Figure 5, one can see that the monodromy matrix

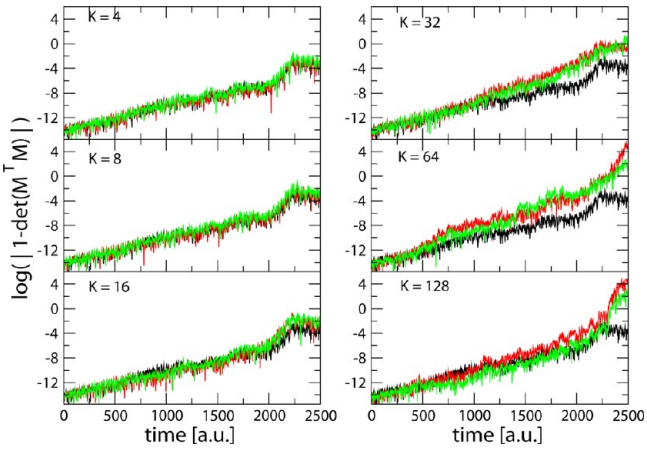

Figure 5. The same as in Figure 1, but for the Henon–Heiles potential. The chaotic parameter is $\lambda = 0.0032$ au.

deviation is more significant for the potential in eq 15 as compared to those for H_2O and CO_2, even when no approximation to the Hessian matrix is applied. Nevertheless, both CFD approximations are quite accurate up to K equals 16. In light of these results, we can assert that the accuracy of both the CFD-Bofill and CFD-PSB approximations is not significantly perturbed by the chaotic motions, and they are robust enough to properly describe the dynamics of complex molecular systems. As a further test, a comparison of the monodromy matrix determinant deviation calculated when using the numerical finite difference algorithm versus the analytical Hessian showed that the differences are within rounding errors and that the deviation from unity is mainly due to the chaotic nature of the potential.

4.2. Direct Dynamics. Ab initio direct dynamics simulations were performed with VENUS[94,95] interfaced with NWChem.[96] Using a development version of the VENUS/NWChem package, simulations were performed with the monodromy matrix calculated at each time step. Simulations were performed for both CO_2 and benzene, using B3LYP/cc-pVDZ theory used for CO_2 and HF/6-31G* for benzene. The same criterion for SCF convergence in the electronic structure theory calculations was used for both molecules and is set to 500 maximum iterations. The Hessian is calculated directly in NWChem by an "analytic" linear algebra algorithm. In a simulation, an ab initio Hessian is calculated once every K time steps, followed by $K - 1$ approximated Hessians. The value for

K was varied, and the trajectories were calculated using Cartesian coordinates.

Figure 6 describes deviations of the CO_2 monodromy matrix determinant from unity for simulations with the CFD-Bofill

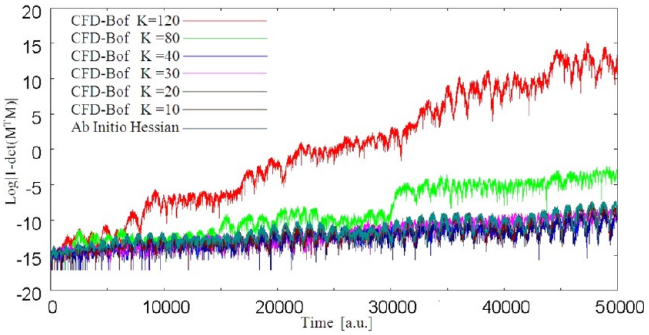

Figure 6. Monodromy matrix determinant deviation from unity for CO_2 direct dynamics simulations. The gray line is for the ab initio Hessian calculation at each time step and the other colors for the CFD-Bofill approximation at different values of K.

approximation for the Hessian. It is important to note that the determinant deviations calculated directly from electronic structure theory with and without any approximation span the same range of values as for the above simulation with the analytic potential function. Thus, both the ab initio theory and analytic function give similar representations of the CO_2 PES. Another similarity between the direct dynamics and analytic potential simulations is given by the relative accuracies of the two CFD approximations.

The deviation of the monodromy determinant from unity for CO_2 is shown in Figure 7 for the CFD-PSB approximation to

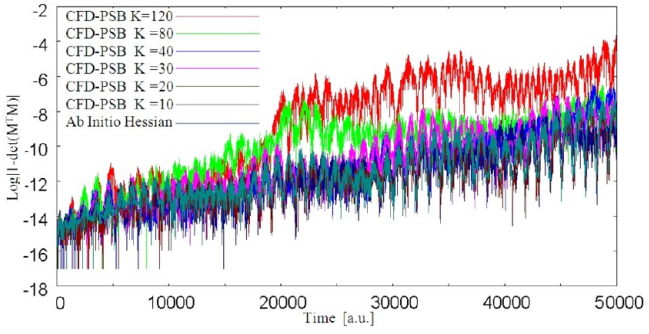

Figure 7. The same as in Figure 6, but for the CFD-PSB Hessian approximation.

the Hessian. By comparing Figures 6 and 7, it is apparent that the CFD-PSB approximation is more accurate than the CFD-Bofill one. The CFD-Bofill approximation can be employed until K equals 40. Below this value, the approximated Hessians are clearly not distinguishable from the exact one.

In contrast to the CFD-Bofill approximation, as shown in Figure 7, the CFD-PSB approximation is accurate up to a K of 120. For a direct dynamics simulation in which the Hessian is determined, the overwhelming computational time is spent for the Hessian calculation. Thus, the CFD-PSB approximation gives a more than two orders of magnitude savings in computational time as compared to calculating the Hessian at each integration step.

Deviations of the benzene monodromy determinant from unity are shown in Figures 8 and 9 for direct dynamics simulations

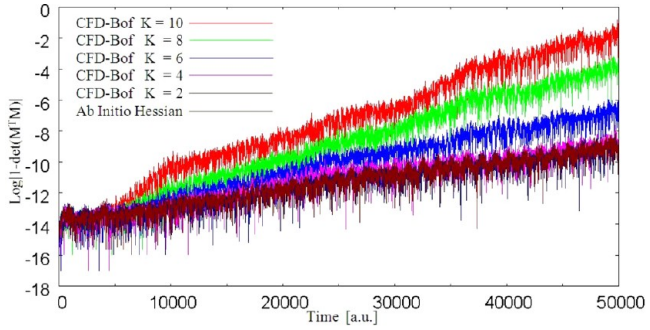

Figure 8. The same as in Figure 6, but for the benzene molecule.

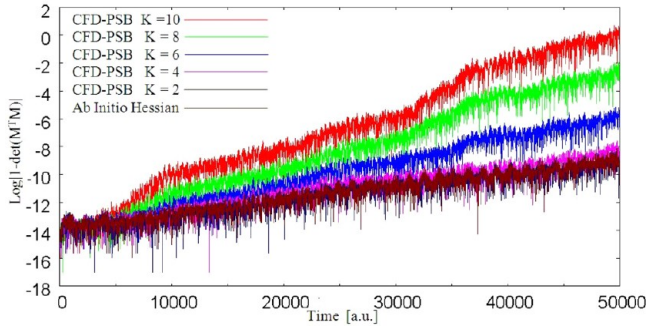

Figure 9. The same as in Figure 8, but for the CFD-PSB Hessian approximation.

utilizing the CFD-Bofill and CFD-PSB approximations, respectively. Benzene has different kinds of couplings, ranging from strong to small, Fermi resonances, and both stiff and floppy modes.[97] There are 30 normal coordinate vibrational degrees of freedom with frequencies ranging from several hundred wavenumbers for out-of-plane and low frequency in-plane modes up to 3000 wave numbers for the C−H stretching modes. Such a variety of modes represents a challenge for the CFD approximation, since the Hessian is approximated using the same 10 au time interval for floppy as well as stiff modes.

As shown in Figure 8, the deviations of the monodromy determinant from unity are substantially larger than those for CO_2 at the same value of K. The CFD-Bofill approximation for benzene gives determinant deviations from unity of approximately 10^{-9}, 10^{-7}, and 10^{-4} at a time of 50 000 au for a K of 4, 6, and 8, respectively. The results for a K of 2 and 4 are nearly identical to those obtained with the ab initio Hessian calculated at each integration step. The results for the CFD-PSB approximation are shown in Figure 9.

The deviation of the monodromy determinant from unity at a time of 50 000 au is 10^{-9}, 10^{-6}, and 10^{-3} for a K of 4, 6, and 8. Comparing Figures 8 and 9 shows that for benzene the CFD-PSB approximation is not more accurate than the CFD-Bofill one, with the latter slightly more accurate for the larger K. For these simulations, one can consider K = 8 as a limiting value for sufficiently accurate results, which gives the velocity Verlet integration algorithm results an approximate 15-fold savings of computational time.

5. SUMMARY

There are a number of important findings from the simulation results presented here. From Figures 1−3, it is apparent that a

dx.doi.org/10.1021/ct300573h | J. Chem. Theory Comput. 2013, 9, 54−64

higher order integration algorithm does not enhance the amount of symplecticity in the dynamics simulation. The reasons for this result are contained in the procedure followed to construct a geometric integration algorithm. The maps are equivalently symmetric for these algorithms, giving rise to their near identical symplecticities.

The simulations for CO_2 based on the analytic potential energy function and those utilizing direct dynamics give very similar deviations of the monodromy matrix determinant from unity. This suggests that the irreversible and nonlinear nature of the SCF optimization for the direct dynamics is not inducing any additional deviation in the monodromy determinant. In contrast, it has been found that these properties of the SCF optimization may lead to significant deviations in the energy conservation.[55,57−62]

The Hamiltonians for the 10-dimensional Henon−Heiles analytic potential function and for benzene direct dynamics model are complex with many nonlinear couplings. The CFD Hessian approximations are found to be robust and suitable for simulations of these systems. The CFD approximation parameter K may be increased or decreased, depending on the level of accuracy required for a specific simulation. Finally, for all the simulations except those for CO_2 direct dynamics, the CFD-Bofill Hessian approximation was found to be more accurate than the CFD-PSB one.

In conclusion, this paper presents a series of detailed tests of CFD approximations for the Hessian calculation. The CFD approximations perform equally well for analytic potential function and direct dynamics simulations. For the latter, they can contribute up to 2 orders of magnitude savings in computational time. The CFD approximations are sufficiently robust to deal with strongly coupled (water, carbon dioxide), complex (benzene), and chaotic (Henon−Heiles) systems.

APPENDIX I

In order to integrate the classical trajectories and the monodromy matrix $\mathbf{M}$ in eq 14, we employed symplectic algorithms, such as the second order velocity Verlet method, the fourth-order McLachlan algorithm, and the Blanes II sixth-order geometric algorithm. As reported in the Appendix of the article by Brewer et al.,[98] an explicit symplectic integrator form for eq 14 is given by

$$\mathbf{M}_{\mathbf{pp}}^{k} = \mathbf{M}_{\mathbf{pp}}^{k-1} - b_k \frac{\partial^2 V(\mathbf{q}_{k-1})}{\partial \mathbf{q}_{k-1}^2} \mathbf{M}_{\mathbf{qp}}^{k-1} \tag{16}$$

$$\mathbf{M}_{\mathbf{pq}}^{k} = \mathbf{M}_{\mathbf{pq}}^{k-1} - b_k \frac{\partial^2 V(\mathbf{q}_{k-1})}{\partial \mathbf{q}_{k-1}^2} \mathbf{M}_{\mathbf{qq}}^{k-1} \tag{17}$$

$$\mathbf{M}_{\mathbf{qp}}^{k} = M_{\mathbf{qp}}^{k-1} + a_k \frac{\partial^2 T(\mathbf{p}_k)}{\partial \mathbf{p}_k^2} \mathbf{M}_{\mathbf{pp}}^{k} \tag{18}$$

$$\mathbf{M}_{\mathbf{qq}}^{k} = \mathbf{M}_{\mathbf{qq}}^{k-1} + a_k \frac{\partial^2 T(\mathbf{p}_k)}{\partial \mathbf{p}_k^2} \mathbf{M}_{\mathbf{pq}}^{k} \tag{19}$$

where $k = 1, 2, ..., m$; m is the symplectic integrator order; and the coefficients a_k and b_k are chosen in order to satisfy the integrator time-reversibility and some specified dynamics accuracy criteria of the order $O(\Delta t^n)$ in Δt, with $n \leq m$. A list of coefficients is given in ref 58, and $V(\mathbf{q}_k)$ and $T(\mathbf{p}_k)$ are respectively the potential and the kinetic energy at step k.

If eq 16 is substituted into the right-hand side of eq 18 and eq 17 into the right-hand side of eq 19, then the monodromy matrix at the kth integration step can be expressed in terms of the monodromy matrix at the $(k-1)$th step as

$$\begin{pmatrix} \mathbf{M}_{\mathbf{qq}}^{k} & \mathbf{M}_{\mathbf{qp}}^{k} \\ \mathbf{M}_{\mathbf{pq}}^{k} & \mathbf{M}_{\mathbf{pp}}^{k} \end{pmatrix} = \begin{pmatrix} \mathbf{I} - a_k b_k \dfrac{\partial^2 T(\mathbf{p}_k)}{\partial \mathbf{p}_k^2} \dfrac{\partial^2 V(\mathbf{q}_{k-1})}{\partial \mathbf{q}_{k-1}^2}, & a_k \dfrac{\partial^2 T(\mathbf{p}_k)}{\partial \mathbf{p}_k^2} \\ -b_k \dfrac{\partial^2 V(\mathbf{q}_{k-1})}{\partial \mathbf{q}_{k-1}^2}, & \mathbf{I} \end{pmatrix} \times \begin{pmatrix} \mathbf{M}_{\mathbf{qq}}^{k-1} & \mathbf{M}_{\mathbf{qp}}^{k-1} \\ \mathbf{M}_{\mathbf{pq}}^{k-1} & \mathbf{M}_{\mathbf{pp}}^{k-1} \end{pmatrix} \tag{20}$$

where $\mathbf{I}$ is the $N \times N$ identity matrix, and N is the number of degrees of freedom. Rewriting eq 20 as

$$\begin{pmatrix} \mathbf{M}_{\mathbf{qq}}^{k} & \mathbf{M}_{\mathbf{qp}}^{k} \\ \mathbf{M}_{\mathbf{pq}}^{k} & \mathbf{M}_{\mathbf{pp}}^{k} \end{pmatrix} = \begin{pmatrix} \mathbf{I}, & a_k \dfrac{\partial^2 T(\mathbf{p}_k)}{\partial \mathbf{p}_k^2} \\ \mathbf{0}, & \mathbf{I} \end{pmatrix} \begin{pmatrix} \mathbf{I}, & \mathbf{0} \\ -b_k \dfrac{\partial^2 V(\mathbf{q}_{k-1})}{\partial \mathbf{q}_{k-1}^2}, & \mathbf{I} \end{pmatrix} \times \begin{pmatrix} \mathbf{M}_{\mathbf{qq}}^{k-1} & \mathbf{M}_{\mathbf{qp}}^{k-1} \\ \mathbf{M}_{\mathbf{pq}}^{k-1} & \mathbf{M}_{\mathbf{pp}}^{k-1} \end{pmatrix} \tag{21}$$

and remembering that $\det(\mathbf{A}\cdot\mathbf{B}\cdot\mathbf{C}) = \det(\mathbf{A})\ \det(\mathbf{B})\ \det(\mathbf{C})$, and assuming that $\det(\mathbf{M}^{k-1}) = 1$, eq 21 implies that the monodromy determinant value of unity is preserved for all time steps. Moreover, eq 21 shows that the algorithm is symplectic for any choice of the coefficients a_k and b_k and any form of the kinetic $(\partial^2 T(\mathbf{p}_k))/(\partial \mathbf{p}_k^2)$ and potential $(\partial^2 V(\mathbf{q}_{k-1})/\partial \mathbf{q}_{k-1}^2)$ Hessians.

Clearly, this is true only in principle, i.e., for an infinite machine precision. When dealing with the monodromy matrix evolution with finite precision machines, a round-off error is propagated, and the determinant deviates from one in a way depending on the choice of the a_k and b_k coefficients, $T(\mathbf{p})$ and $V(\mathbf{q})$. Finite machine precision (and the resulting round-off error) also causes the value of det $(\mathbf{M})$ to deviate from unity in another, much more serious, way when the elements of the matrix are large. Recall that the calculation of det $(\mathbf{M})$ involves the summing and differencing of products of the monodromy elements. If these products are larger than, say, 10^{16} for a double precision calculation, the calculated value of the determinant will not be unity but a meaningless, possibly very large, number. Note that this error will occur even if det $(\mathbf{M})$ is numerically exact within machine precision. This is one reason that it is practically impossible to calculate det $(\mathbf{M})$ accurately for long times in a chaotic system.

Our understanding is that the deviations of det $(\mathbf{M})$ from unity obtained in this paper for H_2O and CO_2 are caused by round-off errors resulting from large monodromy elements. The large values for these elements here are not necessarily produced by chaos but by the approximations applied to calculate the Hessian matrix.

dx.doi.org/10.1021/ct300573h | J. Chem. Theory Comput. 2013, 9, 54−64

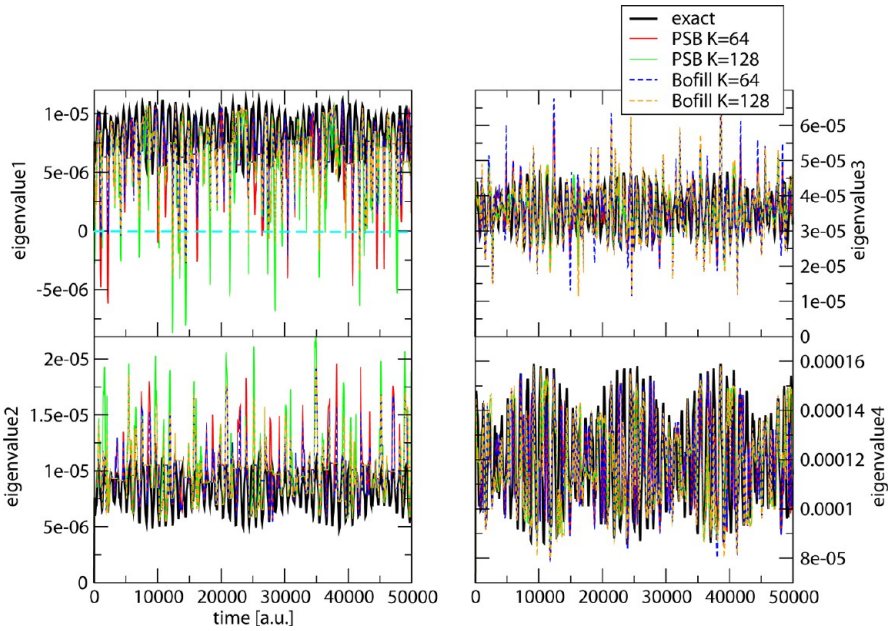

Figure 10. Carbon dioxide Hessian eigenvalues at each time step for several values of K.

To see qualitatively how monodromy elements can become exponentially large, it is convenient to define the modified, but essentially equivalent, monodromy matrix

$$\mathbf{M}' = \begin{pmatrix} \frac{\partial \mathbf{Q}(t)}{\partial \mathbf{Q}(0)} & \frac{\partial \mathbf{Q}(t)}{\partial \mathbf{P}(0)} \\ \frac{\partial \mathbf{P}(t)}{\partial \mathbf{Q}(0)} & \frac{\partial \mathbf{P}(t)}{\partial \mathbf{P}(0)} \end{pmatrix} \tag{22}$$

where $\mathbf{P} = \mathbf{N}^{-1/2}\mathbf{p}$, $\mathbf{Q} = \mathbf{N}^{1/2}\mathbf{q}$, and $\mathbf{N}$ is the diagonal matrix of atomic masses. Then, $\mathbf{M}'$ obeys

$$\frac{d}{dt}\mathbf{M}'(t) = \mathbf{L}\mathbf{M}'(t) \tag{23}$$

where

$$\mathbf{L} = \begin{pmatrix} 0 & \mathbf{I} \\ -\mathbf{H} & 0 \end{pmatrix} \tag{24}$$

and $\mathbf{H}$ is the mass-scaled Hessian matrix calculated at $\mathbf{q}_k$ with elements

$$H_{ij} = \frac{1}{\sqrt{m_i m_j}} \frac{\partial^2 V(\mathbf{q}_k)}{\partial q_{i,k} \partial q_{j,k}} \tag{25}$$

For times Δt that are short enough that $\mathbf{H}$ is almost constant, the solution of this equation is

$$\mathbf{M}'(t + \Delta t) = \exp(\mathbf{L}\Delta t)\, \mathbf{M}'(t) = \mathbf{U} \exp(\Lambda \Delta t)\, \mathbf{U}^{-1}\mathbf{M}'(t) \tag{26}$$

where the diagonal matrix Λ contains the eigenvalues and the matrix $\mathbf{U}$ contains the eigenvectors of $\mathbf{L}$. The diagonal elements λ_j of Λ are obtained by solving the secular equation

$$\det(\mathbf{L} - \lambda \mathbf{1}) = 0 \tag{27}$$

Due to the simple block form of $\mathbf{L}$, this equation can be expressed in terms of N-dimensional determinants as

$$\det(\mathbf{H} + \lambda^2 \mathbf{I}) = 0 \tag{28}$$

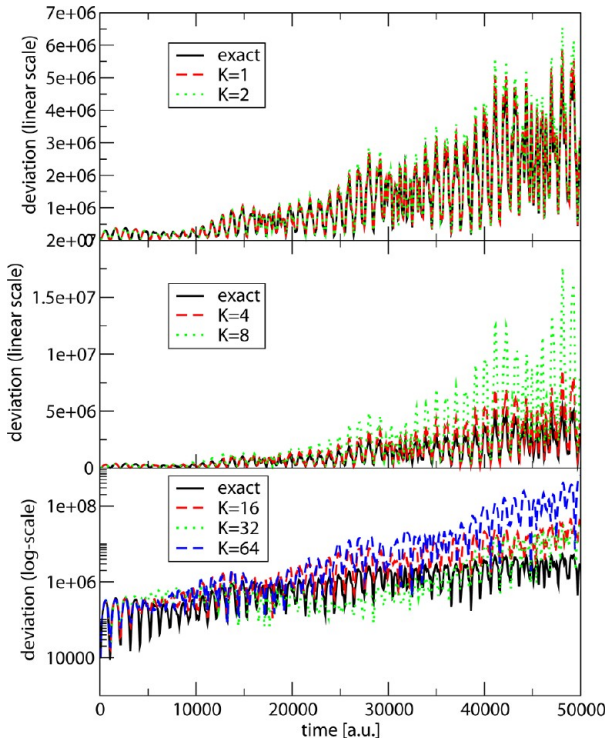

Figure 11. Sum of the square of each monodromy matrix element for the CO_2 dynamics plotted versus time. As the Hessian approximation becomes more severe (larger K values), the monodromy matrix elements become larger in magnitude, and consequentially, their round-off error increases.

which shows that the eigenvalues are given by

$$\lambda_j = \pm i\omega_j \tag{29}$$

where ω_j are the frequencies of the local normal mode coordinates.

Each local mode having a real-valued frequency, corresponding to a positive force constant and a convex up local potential,

dx.doi.org/10.1021/ct300573h | J. Chem. Theory Comput. 2013, 9, 54−64

produces the pair of elements $\exp(\pm i\omega\Delta t)$ in $\exp(\Lambda\Delta t)$. These contribute to bounded oscillating behavior for $\mathbf{M}'(t + \Delta t)$ in eq 23. However, each local mode having an imaginary frequency, corresponding to a negative force constant, produces the pair of elements $\exp(\pm|\omega|\Delta t)$ in $\exp(\Lambda\Delta t)$. These contribute to exponentially increasing and decreasing behavior for the elements of $\mathbf{M}'(t + \Delta t)$. If such imaginary frequencies persist for many intervals Δt, the effects of $\exp(+|\omega|t)$ will dominate, causing at least some of the monodromy elements to increase exponentially.

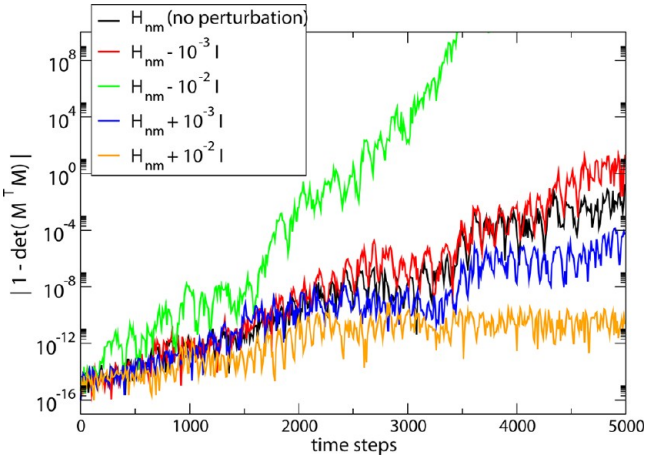

Figure 12. Deviation of $\det(\mathbf{M}^T\mathbf{M})$ from unity by applying the Bofill-CFD approximation at $K = 60$ and with the addition of different fractions of the identity matrix to the approximated Hessian matrix H_{nm}. As the identity matrix positive weight grows, machine precision is approached.

Analyses similar to the one above have been previously applied to predict the onset of chaotic behavior.[99] The exponentially large monodromy elements produced by such chaos leads to substantial round-off error in the calculation of $\det(\mathbf{M})$. We claim that similar results are produced by application of the CFD Hessian approximations for multidimensional systems since the resulting inaccuracies in the calculation of the smallest Hessian eigenvalue can easily make it negative. The more severe the approximation (larger K), the more often the smallest eigenvalue explores negative values. These round-off errors are further enhanced in this paper by the calculation of $\det(\mathbf{M}^T\mathbf{M})$ instead of $\det(\mathbf{M})$.

In Figure 10, the local normal mode eigenvalues are plotted at each time step for the CO_2 trajectory considered in this paper. While the larger eigenvalues are well approximated because of their magnitude, the smallest one is more sensitive to any Hessian approximation.

In this case, as expected, the monodromy matrix elements are found to exponentially increase in magnitude. This is shown in Figure 11, where the sum of the squares of the elements is plotted at different K values, and where one can appreciate (especially from the bottom panel of Figure 11) how the results

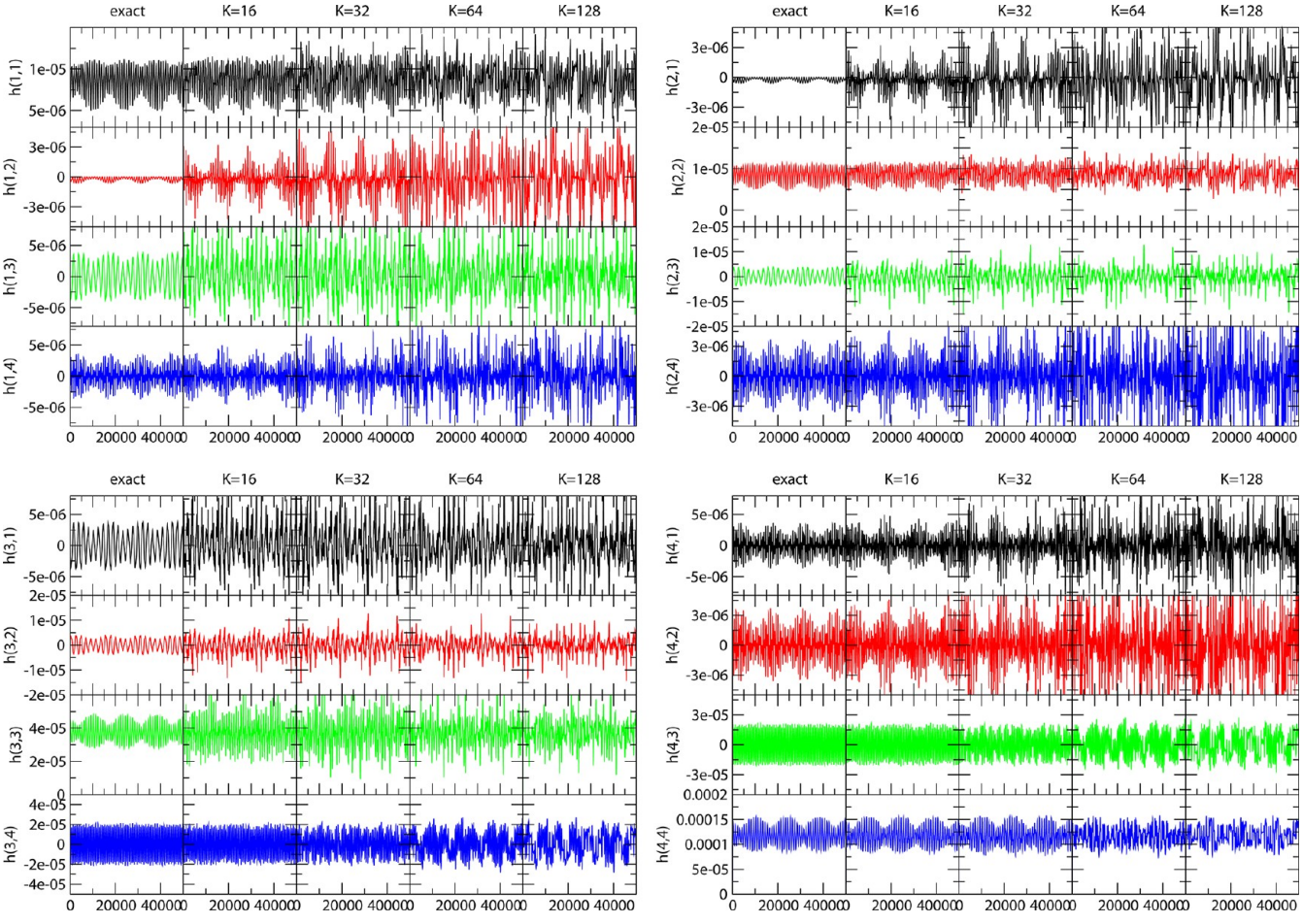

Figure 13. Carbon dioxide Hessian elements at each time step for several values of K.

dx.doi.org/10.1021/ct300573h | J. Chem. Theory Comput. 2013, 9, 54−64

of the Hessian approximations produce monodromy behavior equivalent to the chaos onset in the dynamics of $\mathbf{q}$ and $\mathbf{p}$.

Figure 12 reports results for $\det(\mathbf{M}^T\mathbf{M})$ obtained, as before, by applying the CFD Hessian approximation, but with the addition of the small positive or negative value to each of the diagonal elements of the Hessian matrix at each time step. When positive elements are added, the modification causes the Hessian eigenvalues to become more positive, and it is seen to counteract the exponential rise in the determinant. On the contrary, when negative elements are added, the modification causes the Hessian eigenvalues to become more negative, and deviation of $\det(\mathbf{M}^T\mathbf{M})$ from unity is enhanced. These results support the claim that the large monodromy matrix elements and the large determinants obtained with the CFD approximation are due to the fictitious negative Hessian eigenvalues.

As Figure 13 suggests, the decrease of accuracy in the calculation of $\det(\mathbf{M})$ that results from the CFD approximation can also be related to the loss of regular oscillations of the Hessian diagonal elements and the introduction of fictitious couplings between elements as K is increased. However, an evaluation of the accuracy of the approximation based on such plots is quite arbitrary unless the Hessian is employed for calculating some observable. Monitoring the determinant of the monodromy matrix, as done in this paper, is more useful and convenient than plotting the Hessian elements or the approximated local normal mode eigenvalues, especially for systems that are large or have local Hessian eigenvalues that are negative.

APPENDIX II

In this Appendix, we derive eq 11. Starting from eq 9 and assuming the Hamiltonian of eq 10, one obtains the following equations

$$\frac{d}{dt}\delta\mathbf{p}_t = -\delta\left(\frac{\partial H}{\partial \mathbf{q}}\right)_t \tag{30}$$

$$\frac{d}{dt}\delta\mathbf{q}_t = +\delta\left(\frac{\partial H}{\partial \mathbf{p}}\right)_t \tag{31}$$

where Hamilton's equations have been employed. If one considers a deviation $\delta\mathbf{q}$, the corresponding Hamiltonian deviation is

$$\frac{\partial H}{\partial \mathbf{q}} = \frac{\partial H}{\partial \mathbf{q}}\bigg|_{\mathbf{q}=\mathbf{q}_\circ} + \frac{\partial^2 H}{\partial \mathbf{q}^2}\bigg|_{\mathbf{q}=\mathbf{q}_\circ}\delta\mathbf{q} \tag{32}$$

then the right-hand side of eq 30 is

$$\delta\left(\frac{\partial H}{\partial \mathbf{q}}\right)_t = \frac{\partial^2 H}{\partial \mathbf{q}^2}\delta\mathbf{q}_t \tag{33}$$

and eq 30 becomes

$$\frac{d}{dt}\delta\mathbf{p}_t = -\frac{\partial^2 V}{\partial \mathbf{q}^2}\delta\mathbf{q}_t \tag{34}$$

In the same fashion, eq 31 becomes the following equality

$$\frac{d}{dt}\delta\mathbf{q}_t = \frac{\partial^2 H}{\partial \mathbf{p}^2}\delta\mathbf{p}_t = \frac{1}{m}\delta\mathbf{p}_t \tag{35}$$

and eqs 34 and 35 can be written in the vectorial representation of eq 11.

AUTHOR INFORMATION

Corresponding Author

*E-mail: yu.zhuang@ttu.edu; michele.ceotto@unimi.it.

Notes

The authors declare no competing financial interest.

ACKNOWLEDGMENTS

The University of Milan is thanked for funding (PUR grant) and CILEA (Consorzio Interuniversitario Lombardo per L'Elaborazione Automatica) for computational time allocations. The Texas Tech contribution to this rsearch is based upon work supported by the National Science Foundation under Grant Nos. CHE-0957521 and OISE-0730114 and the Robert A. Welch Foundation under Grant No. D-0005. Support was also provided by the High Performance Computing Center (HPCC) at Texas Tech University, under the direction of Philip W. Smith. Heng Wu, a student of Y.Z., is thanked for helping to plot four figures.

REFERENCES

(1) Bunker, D. L. *Meth. Comput. Phys.* **1971**, *10*, 287−325.
(2) Peslherbe, G. H.; Wang, H.; Hase, W. L. *Adv. Chem. Phys.* **1999**, *105*, 171−201.
(3) Allen, M. D.; Tildesley, D. J. *Computer Simulation of Liquids*; Oxford, NY, 1987; pp 71−108.
(4) Voth, G. A. *Acc. Chem. Res.* **2006**, *39*, 143−150.
(5) Sun, L.; Hase, W. L. *Rev. Comput. Chem.* **2003**, *19*, 79−146.
(6) Sun, L.; Song, K. Y.; Hase, W. L. *Science* **2002**, *296*, 875−878.
(7) Doubleday, C.; Bolton, K.; Peslherbe, G. H.; Hase, W. L. *J. Am. Chem. Soc.* **1996**, *118*, 9922−9931.
(8) Li, G. S.; Hase, W. L. *J. Am. Chem. Soc.* **1999**, *121*, 7124−7129.
(9) Mann, D. J.; Hase, W. L. *J. Am. Chem. Soc.* **2002**, *124*, 3208−3209.
(10) Park, K.; Song, K.; Hase, W. L. *Int. J. Mass Spectrom.* **2007**, *265*, 326−336.
(11) Ceotto, M.; Ayton, G. S.; Voth, G. A. *J. Chem. Theory Comput.* **2008**, *4*, 560−568.
(12) Tu, K. C.; Klein, M. L.; Tobias, D. J. *Biophys. J.* **1998**, *75*, 2147−2156.
(13) Saiz, L.; Klein, M. L. *Acc. Chem. Res.* **2002**, *35*, 482−489.
(14) Bolhuis, P. G.; Chandler, D.; Dellago, C. *Annu. Rev. Phys. Chem.* **2002**, *53*, 291−318.
(15) Liu, P.; Kim, B.; Friesner, R. A. *Proc. Natl. Acad. Sci. U. S. A.* **2005**, *102*, 13749−13754.
(16) Ben-Nun, M.; Martinez, T. J. *Adv. Chem. Phys.* **2002**, *121*, 439−512.
(17) Levine, B. G.; Coe, J. D.; Virshup, A. M.; Martinez, T. J. *Chem. Phys.* **2008**, *347*, 3−16.
(18) Coe, J. D.; Levine, B. G.; Martinez, T. J. *J. Phys. Chem.* **2007**, *111*, 11302−11310.
(19) Schlegel, H. B.; Iyengar, S. S.; Li, X. S.; Millam, J. M.; Voth, G. A.; Scuseria, G. E.; Frisch, M. J. *J. Chem. Phys.* **2002**, *117*, 8694−8704.
(20) Voth, G. A. *Adv. Chem. Phys.* **1996**, *93*, 135−218.
(21) Miller, T. F., III; Manolopoulos, D. *J. Chem. Phys.* **2005**, *122*, 184503.
(22) Craig, I. R.; Manolopoulos, D. E. *J. Chem. Phys.* **2005**, *122*, 084106.
(23) Marx, D.; Parrinello, M. *J. Chem. Phys.* **1996**, *104*, 4077−4082.
(24) Witt, A.; Ivanov, S. D.; Shiga, M.; Forbert, H.; Marx, D. *J. Chem. Phys.* **2009**, *130*, 194510.
(25) Tuckerman, M. E.; Marx, D.; Klein, M. L.; Parrinello, M. *J. Chem. Phys.* **1996**, *104*, 5579−5588.
(26) Iftimie, R.; Minary, P.; Tuckerman, M. E. *Proc. Natl. Acad. Sci. U. S. A.* **2005**, *102*, 6654−6659.
(27) Miller, W. H. *J. Phys. Chem. A* **1998**, *102*, 793−806.

(28) Miller, W. H. *Proc. Natl. Acad. Sci. U. S. A.* **2005**, *102*, 6660−6664.
(29) Heller, E. J. *Acc. Chem. Res.* **1981**, *14*, 368−375.
(30) Heller, E. J. *Acc. Chem. Res.* **2006**, *39*, 127−134.
(31) Kay, K. G. *Annu. Rev. Phys. Chem.* **2005**, *56*, 255−280.
(32) Pollak, E. *J. Chem. Phys.* **2007**, *127*, 074505.
(33) Herman, M. F. *Annu. Rev. Phys. Chem.* **1994**, *45*, 83−111.
(34) Li, B. Q.; Mollica, C.; Vanicek, J. *J. Chem. Phys.* **2009**, *131*, 041101.
(35) Zimmermann, T.; Ruppen, J.; Li, B.; Vaníček, J. *Int. J. Quantum Chem.* **2010**, *110*, 2426−2435.
(36) Shalashilin, D. V.; Child, M. S. *Chem. Phys.* **2004**, *304*, 103−120.
(37) Shalashilin, D. V.; Child, M. S. *J. Chem. Phys.* **2001**, *115*, 5367−5375.
(38) Thoss, M.; Wang, H. *Annu. Rev. Phys. Chem.* **2004**, *55*, 299−332.
(39) Tully, J. C. *Faraday Discuss.* **1998**, *110*, 407−419.
(40) Sholl, D. S.; Tully, J. C. *J. Chem. Phys.* **1998**, *109*, 7702−7710.
(41) Burant, J. C.; Tully, J. C. *J. Chem. Phys.* **2000**, *112*, 6097−6103.
(42) Frantsuzov, P. A.; Mandelshtam, V. A. *J. Chem. Phys.* **2004**, *121*, 9247−9256.
(43) Forest, E.; Ruth, R. D. *Physica D* **1990**, *43*, 105−117.
(44) Yoshida, H. *Phys. Lett. A* **1990**, *150*, 262−268.
(45) Chin, S. A. *Phys. Lett. A* **1997**, *226*, 344−348.
(46) Omelyan, I. P.; Mryglod, I. M.; Folk, R. *Comput. Phys. Commun.* **2003**, *151*, 272−314.
(47) Landau, L. D.; Lifshits, E. M. *Mechanics*; Butterworth: Oxford, U. K., 1976; pp 131−167.
(48) Gutzwiller, M. C. *Chaos in Classical and Quantum Mechanics*; Springer-Verlag: New York, 1991; pp 1−29.
(49) Ceotto, M.; Hase, W. L.; Zhuang, Y. Manuscript in preparation.
(50) Car, R.; Parrinello, M. *Phys. Rev. Lett.* **1985**, *55*, 2471−2474.
(51) Marx, D.; Hutter, J. *Modern Methods and Algorithms of Quantum Chemistry*, 2nd ed.; Grotendorst, J., Ed; John von Neumann Institute for Computing: Julich, Germany, 2000; pp 329−477.
(52) Herbert, J. M.; Head-Gordon, M. *Phys. Chem. Chem. Phys.* **2005**, *7*, 3269−3275.
(53) Li, X.; Tully, J. C.; Schlegel, H. B.; Frisch, M. J. *J. Chem. Phys.* **2005**, *123*, 084106.
(54) Isborn, C. M.; Li, X.; Tully, J. C. *J. Chem. Phys.* **2007**, *126*, 134307.
(55) Niklasson, A. M. N.; Tymczak, C. J.; Challacombe, M. *Phys. Rev. Lett.* **2006**, *97*, 123001.
(56) Pulay, P.; Fogarasi, G. *Chem. Phys. Lett.* **2004**, *386*, 272−278.
(57) Niklasson, A. M. N.; Tymczak, C. J.; Challacombe, M. *J. Chem. Phys.* **2007**, *126*, 144103.
(58) Odell, A.; Delin, A.; Johansson, B.; Bock, N.; Challacombe, M.; Niklasson, A. M. N. *J. Chem. Phys.* **2009**, *131*, 244106.
(59) Odell, A.; Delin, A.; Johansson, B.; Cawkwell, M. J.; Niklasson, A. M. N. *J. Chem. Phys.* **2011**, *135*, 224105.
(60) Niklasson, A. M. N. *Phys. Rev. Lett.* **2008**, *100*, 123004.
(61) Steneteg, P.; Abrikosov, I. A.; Weber, V.; Niklasson, A. M. N. *Phys. Rev. B* **2010**, *82*, 075110.
(62) Niklasson, A. M. N.; Steneteg, P.; Odell, A.; Bock, N.; Challacombe, M.; Tymczak, C. J.; Holmström, E.; Zheng, G.; Weber, V. *J. Chem. Phys.* **2009**, *130*, 214109.
(63) Tangney, P. *J. Chem. Phys.* **2006**, *124*, 044111.
(64) Payne, M. C.; Teter, M. P.; Allan, D. C.; Arias, T. A.; Joannopoulos, J. D. *Rev. Mod. Phys.* **1992**, *64*, 1045−1097.
(65) Wentzcovitch, R. M.; Martins, J. L. *Solid State Commun.* **1991**, *78*, 831−834.
(66) Ceotto, M.; Atahan, S.; Shim, S.; Tantardini, G. F.; Aspuru-Guzik, A. *Phys. Chem. Chem. Phys.* **2009**, *11*, 3861−3867.
(67) Ceotto, M.; Atahan, S.; Tantardini, G. F.; Aspuru-Guzik, A. *J. Chem. Phys.* **2009**, *130*, 234113.
(68) Tatchen, J.; Pollak, E. *J. Chem. Phys.* **2009**, *130*, 041103.
(69) Ceotto, M.; Dell'Angelo, D.; Tantardini, G. F. *J. Chem. Phys.* **2010**, *133*, 054701.
(70) Ceotto, M.; Valleau, S.; Tantardini, G. F.; Aspuru-Guzik, A. *J. Chem. Phys.* **2011**, *134*, 234103.
(71) Wong, S. Y. Y.; Benoit, D. M.; Lewerenz, M.; Brown, A.; Roy, P. -N. *J. Chem. Phys.* **2011**, *134*, 094110.
(72) Ceotto, M.; Tantardini, G. F.; Aspuru-Guzik, A. *J. Chem. Phys.* **2011**, *135*, 214108.
(73) Gelabert, R.; Giménez, X.; Thoss, M.; Wang, H.; Miller, W. H. *J. Phys. Chem. A* **2000**, *104*, 10321−10327.
(74) Broyden, C. G. *Math. Comput.* **1965**, *19*, 577−593.
(75) Powell, M. J. D. *Math. Program.* **1971**, *1*, 26−57.
(76) Dennis, J. E., Jr.; Moré, J. J. *SIAM Rev.* **1977**, *19*, 46−89.
(77) Dennis, J. E. Jr.; Schnabel, R. B. *Numerical Methods for Unconstrained Optimization and Nonlinear Equations*; Prentice Hall: New Jersey, 1983.
(78) Nocedal, J. *Acta Numer.* **1992**, *1*, 199−242.
(79) Bofill, J. M. *J. Comput. Chem.* **1994**, *15*, 1−11.
(80) Bakken, V.; Millam, J. M.; Schlegel, H. B. *J. Chem. Phys.* **1999**, *111*, 8773−8777.
(81) Hratchian, H. P.; Schlegel, H. B. *J. Chem. Theory Comput.* **2005**, *1*, 61−69.
(82) Wu, H.; Rahman, M.; Wang, J.; Lourderaj, U.; Hase, W. L.; Zhuang, Y. *J. Chem. Phys.* **2010**, *133*, 074101.
(83) Lourderaj, U.; Song, K.; Windus, T. L.; Zhuang, Y.; Hase, W. L. *J. Chem. Phys.* **2007**, *126*, 044105.
(84) Lele, S. *J. Comput. Phys.* **1992**, *103*, 16−42.
(85) Lynch, R. E.; Rice, J. R. *Proc. Natl. Acad. Sci.* **1978**, *75*, 2541−2544.
(86) Singer, I.; Turkel, E. *Comput. Meth. Appl. Mech. Eng.* **1998**, *163*, 343−358.
(87) Zhuang, Y.; Sun, X. -H. *Adv. Eng. Software* **2000**, *31*, 585−591.
(88) Zhuang, Y.; Sun, X. -H. *J. Comput. Phys.* **2001**, *171*, 79−94.
(89) Verlet, L. *Phys. Rev.* **1967**, *159*, 98−103.
(90) McLachlan, R. I.; Atela, P. *Nonlinearity* **1992**, *5*, 541−562.
(91) Blanes, S.; Moan, P. C. *J. Comput. Appl. Math.* **2002**, *142*, 313−330.
(92) Dressler, S.; Thiel, W. *Chem. Phys. Lett.* **1997**, *273*, 71−78.
(93) Brewer, M. L. *J. Chem. Phys.* **1999**, *111*, 6168−6170.
(94) Hase, W. L.; Duchovic, R. J.; Hu, X.; Komornicki, A.; Lim, K. F.; Lu, D.; Peslherbe, G. H.; Swamy, K. N.; Vande Linde, S. R.; Varandas, A.; Wang, J.; Wolf, R. J. *Quant. Chem. Program Exch. (QCPE) Bull.* **1996**, *16*, 671.
(95) Hu, X.; Hase, W. L.; Pirraglia, T. *J. Comput. Chem.* **1991**, *12*, 1014−1024.
(96) Valiev, M.; Bylaska, E. J.; Govind, N.; Kowalski, K.; Straatsma, T. P.; van Dam, H. J. J.; Wang, D.; Nieplocha, J.; Apra, E.; Windus, T. L.; de Jong, W. A. *Comput. Phys. Commun.* **2010**, *181*, 1477−1489.
(97) Senent, M.-L.; Palmieri, P.; Carter, S.; Handy, N. C. *Chem. Phys. Lett.* **2002**, *354*, 1−8.
(98) Brewer, M. L.; Hulme, J. S.; Manolopoulos, D. E. *J. Chem. Phys.* **1997**, *106*, 4832−4839.
(99) Brumer, P.; Duff, J. W. *J. Chem. Phys.* **1976**, *65*, 3566. Duff, J. W.; Brumer, P. *J. Chem. Phys.* **1977**, *67*, 4898. Brumer, P. *J. Comput. Phys.* **1973**, *14*, 391. Hinde, R. J.; Berry, R. S.; Wales, D. J. *J. Chem. Phys.* **1992**, *96*, 1376. Wales, D.; Berry, R. S. *J. Phys. B: At. Mol. Opt. Phys.* **1991**, *24*, L351−L357. Kosloff, R.; Rice, S. A. *J. Chem. Phys.* **1981**, *74*, 1947. Toda, M. *Phys. Lett. A* **1974**, *48*, 335. Cerjan, C.; Reinhardt, W. P. *J. Chem. Phys.* **1979**, *71*, 1819 and others.